



Coverage analysis of ultra-dense heterogeneous cellular networks with interference management

Muhammad Sajid Haroon¹ · Ziaul Haq Abbas¹ · Ghulam Abbas¹ · Fazal Muhammad²

Published online: 27 February 2019
© Springer Science+Business Media, LLC, part of Springer Nature 2019

Abstract

Deploying ultra-dense small base stations (SBSs) in the coverage umbrella of a macro base station (MBS) requires proactive users offloading from MBS to SBSs to achieve maximum performance gain in heterogeneous cellular networks. However, it degrades the signal-to-interference-plus-noise ratio (SINR) of the offloaded users due to strong interference received from MBS. To improve users' SINR, an efficient interference mitigation scheme is required to be used in conjunction with users offloading. Soft frequency reuse (SFR) is an attractive and spectrally efficient interference mitigation scheme that allocates available bandwidth among all cell users associated with k BS, where $k \in (M, S)$. To address the problem of interference, we use the SFR scheme together with power control factor (β) to transmit at different power levels for interior and edge regions of k BS, i.e., r_k^i and r_k^e , respectively. We further consider uniform and nonuniform SBS distribution in the premises of MBS and analyse the effect of the SFR scheme on the proposed model with the help of Stochastic geometry. Mathematical expressions for coverage probabilities are derived and validated through simulations. Numerical results show that the proposed model achieves better coverage probability due to reduced interference. Moreover, nonuniform SBS distribution together with the SFR scheme further improves the performance gain of the proposed model.

Keywords Stochastic geometry · Poisson point processes · Nonuniform SBS distribution · SFR scheme · Nakagami-m fading · Coverage probability

1 Introduction

The demand for ubiquitous coverage with high data rates is increasing exponentially, which forces the cellular network operators to increase the capacity as well as improve the efficiency of networks. Mobile data usage has increased by 200% in recent years [2]. One of the cost effective and efficient schemes for increasing the network capacity is the

ultra-dense deployment of small base stations (SBSs) inside the coverage umbrella of a macro base station (MBS) [3]. Poisson point process (PPP) has been extensively used to model and analyse heterogeneous cellular networks (HCNs) due to its tractability and accuracy [4, 5]. MBSs and SBSs are, therefore, spatially distributed using independent PPPs.

In HCNs, a user associates itself with k BS, where $k \in (M, S)$, based on maximum long term received power. An MBS transmits with higher power as opposed to SBSs and, thus, causes more users to get associated with it. This results in an imbalanced user distribution across HCNs and an inefficient resource utilization [6, 7]. To address this problem, the authors in [8] offload users from MBSs to low power SBSs for better resource utilization in HCNs. However, this results in reduce signal-to-interference-plus-noise ratio (SINR) due to strong interference received from offloaded base station, i.e., MBS, and thus acts as a limiting factor for performance gain of HCNs [9]. Hence, a proactive interference abating scheme is required together

A part of this paper has been presented in the 28th International Telecommunication Networks and Applications Conference (ITNAC'2018), in University of New South Wales, Sydney, Australia [1].

✉ Muhammad Sajid Haroon
sajid.haroon@giki.edu.pk

¹ Telecommunications and Networking (TeleCoN) Research Lab, GIK Institute of Engineering Sciences and Technology, Topi 23640, Pakistan

² Department of Electrical Engineering, City University of Science and Information Technology, Peshawar, Pakistan

with the users offloading. In state-of-the-art, one of the potential interference abating schemes is the fractional frequency reuse (FFR) [10], where the entire frequency band, W , of the system is partitioned into small sub-bands to mitigate interference and, thus, improve coverage. However, only a fraction of W is allocated to each tier of BSs, therefore, this scheme proves to be spectrally inefficient. Another such interference abating scheme is the soft frequency reuse (SFR) [11]. SFR is spectrally more efficient, compared with FFR, because all bandwidth is made available for each tier of BSs.

In [12, 13], the authors divide MBS coverage region into two sub-regions, i.e., cell edge region and cell interior region for better coverage analysis. Users located in the edge region experience low SINR due to their distant locations [12]. However, users offloading in the cell interior region encounter severe interference due to close proximity of users to MBS that transmits with high power [13]. Additionally, SBSs in cell interior region have reduced coverage area due to strong signals received from MBS [12].

In [14], analytical models for FFR and SFR schemes, based on spatial PPP, are proposed. Furthermore, tractable expressions for each scheme are derived. The authors show that SFR is spectrally more efficient, whereas FFR provides highest gains in the lowest average SINR scenario. In [15], downlink multichannel model for SFR is analysed along with average user rate. Moreover, optimal combinations of association bias and SFR parameters are investigated. The authors show that SFR outperforms FFR in different load conditions. In [16], general mathematical models are developed for load balancing both with FFR and SFR while considering downlink transmission for HCNs. The authors show that FFR outperforms SFR in terms of SINR and rate coverage. However, it fails to provide the same spectral efficiency as that of SFR. Furthermore, the authors reduce the complex general mathematical expressions to simple closed-forms for rate and coverage analyses. In [17], load balancing together with reverse frequency allocation (RFA) scheme are analysed while considering two tier HCNs. Expressions for coverage probability while assuming both interior and edge regions of MBS are derived. There is significant improvement in coverage by using RFA with load balancing. In [18], RFA along with nonuniform SBS deployment are considered. SBSs are muted in cell interior region while they remain active in cell edge region. Expressions for both coverage probability and average rate are derived. Numerical results indicate that nonuniform SBS deployment in MBS coverage region shows significant improvement in rate coverage. Similarly, in [19] energy efficient user association and power allocation in millimeter wave-based HCNs are proposed while focusing on load balancing, energy

harvesting, quality of service, and interference. Moreover, the complexity of the proposed model is analyzed and compared with existing schemes via simulations.

In this paper, we propose a nonuniform SBS deployment strategy where SBSs provide service to the users in cell edge region, r_M^e , and are assumed to be muted in cell interior region, r_M^i . Furthermore, we employ SFR, which is spectrally more efficient due to availability of entire bandwidth to the users of both MBS and SBSs. The major contributions of this paper are as follows:

- (1) Received SINR of the offloaded users degrades due to strong interference received from MBS. Therefore, we propose SFR employment to effectively mitigate the interference and use the spectrum efficiently.
- (2) To the best of our knowledge, SFR has been studied independently without considering nonuniform SBS distribution scenario. Therefore, we propose a unified model for nonuniform SBS deployment along with SFR to mitigate interference with optimal resource utilization while considering Rayleigh fading as a special case of Nakagami- m distribution.
- (3) Universal bottleneck in cellular networks is the edge user performance due to its distant location from serving BS. The results show that the proposed model reduces interference and, thus, significantly increases edge user performance gain.
- (4) Coverage probability is analysed against signal-to-noise ratio (SNR) value, SINR threshold, and MBS and SBS densities.
- (5) Results demonstrate that the SFR employment together with nonuniform SBS distribution requires fewer SBSs, which results in reduced interference and, hence, improves coverage probability.

The rest of the paper is organized as follows. In Sect. 2, network model for both uniform and nonuniform SBS deployment in MBS coverage area together with SFR is presented. In Sect. 3, coverage probability of the proposed scheme is analysed. In Sect. 4, numerical results are presented with discussion, and Sect. 5, concludes the paper. The notations used in the paper are listed in Table 1.

2 System model

This section focuses on both uniform and nonuniform ultra-dense SBS deployment in the coverage area of MBS along with the SFR scheme and Nakagami- m fading. Furthermore, we develop mathematical preliminaries, which will be used in Sect. 3 to derive coverage probability expressions.

Table 1 Notation summary

Parameter	Description
Ψ_k	PPPs of k BS locations, $\forall k \in (M, S)$
σ^2	Noise power
U	Uniform SBS distribution scenario
NU	Nonuniform SBS distribution scenario
η_k	SNR_k values
$P_{t,k}$	Power transmitted by k BS
ρ_k, ρ_τ	Density of k BS and τ BS, respectively
P_r	Power received from serving BS
α	Path loss exponents for k BS where $\alpha > 2$
γ_k	SINR threshold of k BS
Γ_k	SINR received by T_u from k BS
r_k^i, r_k^e	Interior and edge regions of k BS, $\forall k \in (M, S)$
x_k, y_τ	Statistical distances of associated k BS and τ BS to the T_u , respectively
β	Power control factor
S	Distance between k BS and user
$R(U)$	Region for uniform SBS deployment, s.t., $R(U) = \bigcup_{j \in \{i, e\}} r_M^j$
$R(NU)$	Region for nonuniform SBS deployment, s.t., $R(NU) = r_M^e$
$\rho_S^{R(U)}$	SBS density in $R(U)$
$\rho_S^{R(NU)}$	SBS density in $R(NU)$
F	Total available bandwidth
$F^{r_M^i}, F^{r_M^e}$	Sub-bands for r_M^i and r_M^e , respectively
$F^{r_S^i}, F^{r_S^e}$	Sub-bands for r_S^i and r_S^e , respectively
$d_1^{r_M^i}, d_2^{r_M^e}$	Coverage limits for interior and exterior regions of MBS
$d_1^{r_S^i}, d_2^{r_S^e}$	Coverage limits for interior and exterior regions of SBS
h_x	Fading parameter, following Nakagami- m distribution
$P_{k,D_L}^{r_c}(\gamma_k, U)$	D_L coverage probability for uniform SBS distribution
$P_{k,U_L}^{r_c}(\gamma_k, U)$	U_L coverage probability for uniform SBS distribution
$P_{k,D_L}^{r_c}(\gamma_k, NU)$	D_L coverage probability for nonuniform SBS distribution
$P_{k,U_L}^{r_c}(\gamma_k, NU)$	U_L coverage probability for nonuniform SBS distribution

2.1 Network model

We consider two tier network model, where SBSs are overlaid in the coverage region of MBS to increase network capacity. SFR is used to mitigate interference caused

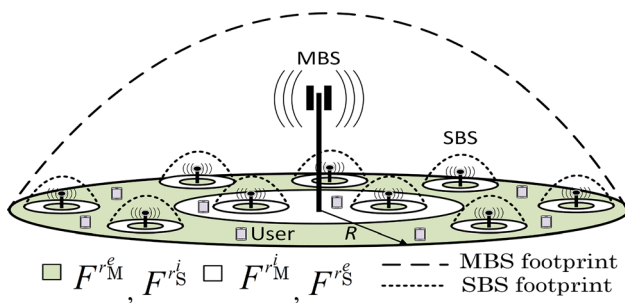


Fig. 1 SBS deployment scenario using SFR

by user offloading. Figure 1 shows the multi-tier BSs deployment along with SFR. Here R denotes the radius for entire coverage region of MBS. Coverage region of each tier is divided into two sub-regions, i.e., interior region, r_c^i , and edge region r_c^e where $c \in (M, S)$. Moreover, due to SFR employment, the frequencies used by MBS in r_M^i and r_M^e are used by SBS in r_S^e and r_S^i , respectively. According to SFR, total bandwidth F is divided into two identical sub-bands $F^{r_c^i}$ and $F^{r_c^e}$ [14], where $\tau \in (M, S)$ and $k \in (M, S) \forall \tau \neq k$, s.t., $F^{r_c^i} = F^{r_c^e}$ and $F^{r_c^i} \cap F^{r_c^e} = \phi$, as shown in Table 2. The SFR sub-bands are used in alternate regions by k BS and τ BS, s.t., complete frequency band $F = F^{r_c^i} \cup F^{r_c^e}$ [15]. We consider a two-tier cellular network model employing SFR while assuming uniform and nonuniform SBS deployment scenarios as shown in Figs. 2 and 3, respectively. MBSs are considered as first tier, while

Table 2 Frequency distribution using SFR

BS	Edge region (r_k^e)	Interior region (r_k^i)
k BS	$F^{r_k^e}$	$F^{r_k^i}$
τ BS	$F^{r_k^e}$	$F^{r_k^i}$

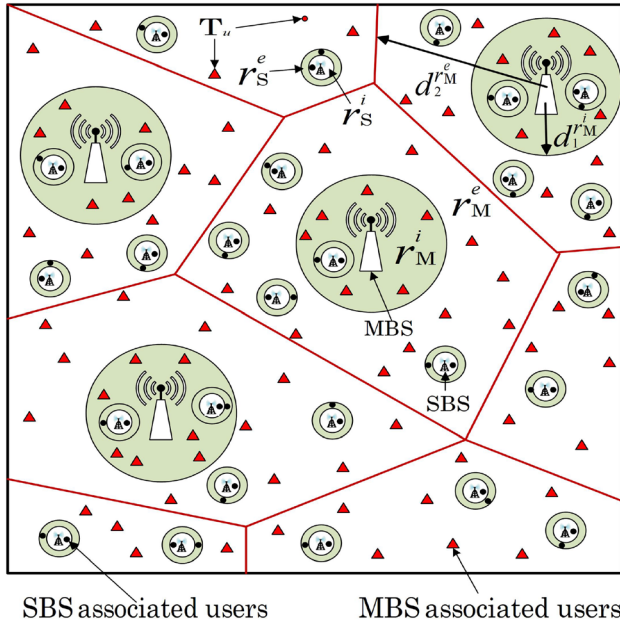


Fig. 2 Ultra-dense uniform SBS deployment scenario using SFR. Here triangles denote the users associated with MBS and dots denote the users associated with SBS

SBSs as second tier. MBS, SBSs and users are spatially distributed using independent PPPs, ψ_M , ψ_S , and ψ_u , respectively. For co-channel network deployment, all available sub-channels are shared by both tiers. Analysis are performed on typical user T_u located at the origin, which is allowed by Slivnyak theorem [18]. For the sake of tractability, standard path loss model is assumed with path loss exponent $\alpha > 2$, whereas noise is considered as additive with power σ^2 . Furthermore, we assume that $\alpha_k = \alpha_S = \alpha$. Fading is modeled using Nakagami- m distribution with Rayleigh fading as a special case when $m = 1$. To address coverage issues in cell edge region, r_k^e , we use power control factor, β , to transmit high power in r_k^e as compared to cell interior region, r_k^i , where, $k \in (M, S)$ [14]. Users in r_k^i are served with low transmit power, i.e., βP_t with $\beta = 1$, whereas users in r_k^e are served with high transmit power level, i.e., βP_t with $\beta > 1$.

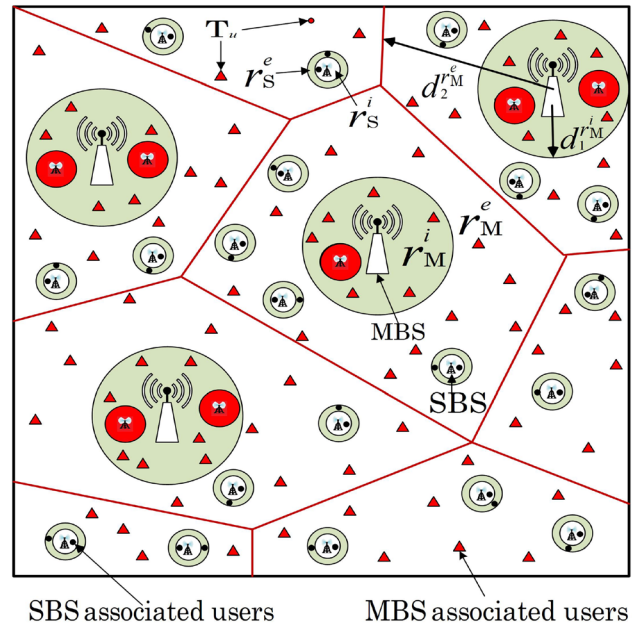


Fig. 3 Ultra-dense uniform SBS deployment scenario using SFR. Here triangles denote the users associated with MBS, dots denote the users associated with SBS and red small circles represents the muted SBSs

2.2 System model with uniform and nonuniform SBS deployment scenario

Coverage areas of each tier BSs are divided into r_k^i and r_k^e with frequency bands distributed using SFR. SBSs are uniformly deployed via PPP with density ρ_S , throughout the coverage area of MBS, as shown in Fig. 2. Similarly, Fig. 3 shows nonuniform SBS distribution scenario where SBSs in r_M^i are muted due to reasonable MBS coverage, severe interference received by offloaded user, reduced SBS coverage and fewer SBS user associations [12, 13]. Here, red circular discs show the muted SBSs. Furthermore, triangles and dots represent the user’s association with MBS and SBSs, respectively, and d_1 and d_2 represent the radii of r_M^i and r_M^e , respectively.

2.3 Downlink and uplink SINR analysis

Downlink (D_L) and uplink (U_L) SINR received at T_u^k and k BS, respectively, while considering both uniform (U) and nonuniform (NU) SBS distribution are calculated, respectively, as

$$\Gamma_{D_L,k}^{r_k^e}(S, U) = \frac{P_{r,D_L,S}}{I_{tot,D_L}^{r_k^e}(U) + \sigma^2}, \tag{1}$$

$$\Gamma_{U_L,k}^{r_k^e}(S, U) = \frac{P_{r,U_L,S}}{I_{tot,U_L}^{r_k^e}(U) + \sigma^2}, \tag{2}$$

$$\Gamma_{D_L,k}^{r_k^e}(\mathcal{S}, NU) = \frac{P_{r,D_L,\mathcal{S}}}{I_{tot,D_L}^{r_k^e}(NU) + \sigma^2}, \tag{3}$$

and

$$\Gamma_{U_L,k}^{r_k^e}(\mathcal{S}, NU) = \frac{P_{r,U_L,\mathcal{S}}}{I_{tot,U_L}^{r_k^e}(NU) + \sigma^2}. \tag{4}$$

Here $\Gamma(\cdot)$ represents the received SINR at T_u , \mathcal{S} denotes the distance between kBS and T_u . $P_{r,D_L,\mathcal{S}}$ is the power received by T_u from kBS in D_L direction, while $P_{r,U_L,\mathcal{S}}$ is the power received by kBS from T_u in U_L direction.

Interference distribution scenarios of T_u associated with kBS while assuming uniform and nonuniform SBS deployment scenarios are given in Tables 3 and 4, respectively. For uniform deployment scenario, SBSs are distributed using independent PPP in the region $R(U)$ of MBS, where $R(U) = \bigcup_{j \in \{i,e\}} r_M^j$ with density $\rho_S^{R(U)} \in \bigcup_{j \in \{i,e\}} r_M^j$. Similarly, for nonuniform deployment scenario, SBSs are randomly distributed using independent PPP in the region $R(NU)$ s.t., $R(NU) = r_M^e$ with $\rho_S^{R(NU)} \in r_M^e$.

Total D_L and U_L interference received at T_u^k , while considering uniform SBS deployment scenario, is the sum of U_L and D_L interference received from users located in r_k^e while associated with kBS and from users located in r_τ^i while associated with τBS . Total D_L and U_L interference, i.e., $I_{tot,D_L}^{r_k^e}(U)$ and $I_{tot,U_L}^{r_k^e}(U)$, are therefore given respectively as

$$I_{tot,D_L}^{r_k^e}(U) = I_{D_L}^{r_k^e} + I_{U_L}^{r_k^e} + I_{D_L}^{r_\tau^i} + I_{U_L}^{r_\tau^i}, \quad \forall \rho_S^{R(U)}, \tag{5}$$

$$I_{tot,U_L}^{r_k^e}(U) = I_{U_L}^{r_k^e} + I_{D_L}^{r_k^e} + I_{U_L}^{r_\tau^i} + I_{D_L}^{r_\tau^i}, \quad \forall \rho_S^{R(U)}. \tag{6}$$

Similarly, total D_L and U_L interference received at T_u^k , i.e., $I_{tot,D_L}^{r_k^e}(NU)$ and $I_{tot,U_L}^{r_k^e}(NU)$, respectively, while considering nonuniform SBS deployment scenario, is the sum of U_L and D_L interference received from users located in r_k^e while associated with kBS and from users located in r_τ^i while associated with τBS , and can be written as

$$I_{tot,D_L}^{r_k^e}(NU) = I_{D_L}^{r_k^e} + I_{U_L}^{r_k^e} + I_{D_L}^{r_\tau^i} + I_{U_L}^{r_\tau^i}, \quad \forall \rho_S^{R(NU)}, \tag{7}$$

$$I_{tot,U_L}^{r_k^e}(NU) = I_{U_L}^{r_k^e} + I_{D_L}^{r_k^e} + I_{U_L}^{r_\tau^i} + I_{D_L}^{r_\tau^i}, \quad \forall \rho_S^{R(NU)}. \tag{8}$$

Here $k \in (M, S)$ and $\tau \in (M, S) \forall k \neq \tau$. $I_{D_L}^{r_k^e}(\cdot)$ is the D_L interference received by T_u^k from kBS , $I_{U_L}^{r_k^e}(\cdot)$ is the U_L interference received by kBS from T_u^k , $I_{D_L}^{r_\tau^i}(\cdot)$ is the D_L interference received by T_u^i from τBS , and $I_{U_L}^{r_\tau^i}(\cdot)$ is the U_L interference received by τBS from T_u^i .

The total interference expressions of Eqs. (5) and (6) can be rewritten as

$$\begin{aligned} I_{tot,D_L}^{r_k^e}(U) &= \sum_{x_k \in \Psi_k^e \setminus d_k} \beta P_{t,D_L}^k h_{x_k}^{r_k^e} \|x_k\|^{-\alpha} + \sum_{y_k \in \Psi_u^e} P_{t,U_L}^u h_{y_k}^{r_k^e} \|y_k\|^{-\alpha} \\ &+ \sum_{x_\tau \in \Psi_\tau^{R(U)}} P_{t,D_L}^\tau h_{x_\tau}^{r_\tau^i} \|x_\tau\|^{-\alpha} + \sum_{y_\tau \in \Psi_u^{r_\tau^i}} P_{t,U_L}^u h_{y_\tau}^{r_\tau^i} \|y_\tau\|^{-\alpha} \vee \rho_S^{R(U)}, \end{aligned} \tag{9}$$

and

$$\begin{aligned} I_{tot,U_L}^{r_k^e}(U) &= \sum_{y_k \in \Psi_u^e \setminus d_k} P_{t,U_L}^u h_{y_k}^{r_k^e} \|y_k\|^{-\alpha} + \sum_{x_k \in \Psi_k^e} \beta P_{t,D_L}^k h_{x_k}^{r_k^e} \|x_k\|^{-\alpha} \\ &+ \sum_{y_\tau \in \Psi_u^{r_\tau^i}} P_{t,U_L}^u h_{y_\tau}^{r_\tau^i} \|y_\tau\|^{-\alpha} + \sum_{x_\tau \in \Psi_\tau^{R(U)}} P_{t,D_L}^\tau h_{x_\tau}^{r_\tau^i} \|x_\tau\|^{-\alpha} \vee \rho_S^{R(U)}. \end{aligned} \tag{10}$$

where x_k is the distance between kBS and users in D_L direction, x_τ is the distance between τBS and users in D_L direction, y_k is the distance between kBS and users in U_L direction, and y_τ is the distance between τBS and users in U_L direction.

Similarly, total D_L and U_L interference received by T_u^k , i.e., $I_{tot,D_L}^{r_k^e}(NU)$ and $I_{tot,U_L}^{r_k^e}(NU)$, while considering nonuniform SBS deployment scenario can be derived in a similar way as Eqs. (9) and (10), and are given by

$$\begin{aligned} I_{tot,D_L}^{r_k^e}(NU) &= \sum_{x_k \in \Psi_k^e \setminus d_k} \beta P_{t,D_L}^k h_{x_k}^{r_k^e} \|x_k\|^{-\alpha} + \sum_{y_k \in \Psi_u^e} P_{t,U_L}^u h_{y_k}^{r_k^e} \|y_k\|^{-\alpha} \\ &+ \sum_{x_\tau \in \Psi_\tau^{R(NU)}} P_{t,D_L}^\tau h_{x_\tau}^{r_\tau^i} \|x_\tau\|^{-\alpha} \\ &+ \sum_{y_\tau \in \Psi_u^{r_\tau^i}} P_{t,U_L}^u h_{y_\tau}^{r_\tau^i} \|y_\tau\|^{-\alpha} \vee \rho_S^{R(NU)}, \end{aligned} \tag{11}$$

and

$$\begin{aligned} I_{tot,U_L}^{r_k^e}(NU) &= \sum_{y_k \in \Psi_u^e \setminus d_k} P_{t,U_L}^u h_{y_k}^{r_k^e} \|y_k\|^{-\alpha} + \sum_{x_k \in \Psi_k^e} \beta P_{t,D_L}^k h_{x_k}^{r_k^e} \|x_k\|^{-\alpha} \\ &+ \sum_{y_\tau \in \Psi_u^{r_\tau^i}} P_{t,U_L}^u h_{y_\tau}^{r_\tau^i} \|y_\tau\|^{-\alpha} \\ &+ \sum_{x_\tau \in \Psi_\tau^{R(NU)}} P_{t,D_L}^\tau h_{x_\tau}^{r_\tau^i} \|x_\tau\|^{-\alpha} \vee \rho_S^{R(NU)}. \end{aligned} \tag{12}$$

Table 3 Interference distribution using SFR for Uniform SBS Deployment

Scenario	T_u location	Interferences received from
$\rho_S^{R(U)} \in \bigcup_{j \in \{i,e\}} r_M^j$	r_M^i	$I_{U_L}^i + I_{D_L}^i + I_{U_L}^e + I_{D_L}^e$
	r_S^i	$I_{U_L}^i + I_{D_L}^i + I_{U_L}^e + I_{D_L}^e$
	r_M^e	$I_{U_L}^e + I_{D_L}^e + I_{U_L}^i + I_{D_L}^i$
	r_S^e	$I_{U_L}^e + I_{D_L}^e + I_{U_L}^i + I_{D_L}^i$

Table 4 Interference distribution using SFR for nonuniform SBS deployment

Scenario	T_u location	Interferences received from
$\rho_S^{R(NU)} \in (r_M^e)$	r_M^i	$I_{U_L}^i + I_{D_L}^i + I_{U_L}^e + I_{D_L}^e$
	r_S^i	$I_{U_L}^i + I_{D_L}^i + I_{U_L}^e + I_{D_L}^e$
	r_M^e	$I_{U_L}^e + I_{D_L}^e + I_{U_L}^i + I_{D_L}^i$
	r_S^e	$I_{U_L}^e + I_{D_L}^e + I_{U_L}^i + I_{D_L}^i$

Equations (9) and (10) are similar to Eqs. (11) and (12), respectively, except the main difference of SBS density, which ultimately reduces interference in nonuniform SBS deployment scenario. Here $h_{x_k}^{r_k^e}$, $h_{y_k}^{r_k^e}$, $h_{x_\tau}^{r_k^i}$ and $h_{y_\tau}^{r_k^i}$ are the fading coefficients that follow Nakagami-m distribution. It is worth mentioning here that Nakagami-m is more suitable to be used for mobile applications [20]. It also has the inherent ability to model a wide variety of other fading environments, such as one-sided Gaussian distribution ($m = 1/2$) and Rayleigh distribution ($m = 1$). It closely matches the Rician distribution ($m > 1$) and no fading ($m = \infty$) [20]. Signals to the users in r_k^e are transmitted with high power, i.e., $\beta P_{t,k}$ where $\beta > 1$, whereas signals to users in r_k^i are fed with low power, i.e., $\beta P_{t,k}$ with power control factor, $\beta = 1$.

2.4 Distribution of statistical distances Y_k between associated k BS to the T_u

Based on the model we have developed above, the distribution of distances Y_k between associated k BS and the T_u is derived in the following.

Considering void probability property of PPP [21, 22], the probabilities that T_u is located in r_M^e and r_M^i , i.e., $P_{T_u^e}^{r_M^e}$ and $P_{T_u^i}^{r_M^i}$, respectively, are

$$P_{T_u^e}^{r_k^e} = \exp\left(-\rho_k \pi (d_1^k)^2\right), \tag{13}$$

and

$$P_{T_u^i}^{r_k^i} = 1 - P_{T_u^e}^{r_k^e} \quad \forall k \in \{M\}. \tag{14}$$

Here $\pi (d_1^k)^2$ and d_1^k denote the area and radius of r_k^i , respectively, with ρ_k represents the k BS density.

Assuming user association scheme, based on maximum received power,¹ PDF of association distances for k BS, located at y_k to the T_u , i.e, $f_{Y_k}(y_k)$, is given as [23]

$$f_{Y_k}(y_k) = 2\pi\rho_k y_k \exp(-\pi\rho_k y_k^2). \tag{15}$$

Similarly, conditional PDF of the distances for T_u in r_k^i and r_k^e of each tier, while associated with k BS, i.e., $f_{Y_k|T_u^i}^{r_k^i}(y_k)$ and $f_{Y_k|T_u^e}^{r_k^e}(y_k)$, are given, respectively, as [24, 25]

$$f_{Y_k|T_u^i}^{r_k^i}(y_k) = \frac{2\pi\rho_k y_k \exp(-\rho_k \pi y_k^2)}{1 - \exp\left(-\rho_M \pi (d_1^M)^2\right)}, \tag{16}$$

and

$$f_{Y_k|T_u^e}^{r_k^e}(y_k) = \frac{2\pi\rho_k y_k \exp(-\rho_k \pi y_k^2)}{\exp\left(-\rho_M \pi (d_1^M)^2\right)}. \tag{17}$$

3 Coverage probability

Definition 1 (Coverage Probability) Downlink coverage probability can be defined as the successful communication between users and associated k BS, provided that received SINR, Γ_k , at user is greater then its predefined threshold, γ_k [26], i.e.,

$$P_{k,D_L}^{r_k^e}(\gamma_k) \triangleq P\left[\Gamma_k^{r_k^e}(y_k) > \gamma_k | T_u^{r_k^e}\right] = E\left[P\left[\Gamma_k^{r_k^e}(y_k) > \gamma_k | T_u^{r_k^e}\right]\right].$$

Users with similar frequency bands in the cell receive increased interference, which ultimately degrades the received SINR and, hence, the coverage probability. In this section, we develop expressions for coverage probability assuming T_u located in r_k^e , while considering both the uniform and nonuniform system models derived in the previous section.

¹ In maximum received power association scheme, a user associates itself with the BS from which it receives maximum long term power as compared to other BSs in the network.

3.1 Coverage probability for uniform SBS distribution scenario

D_L and U_L coverage probabilities of $T_u^{r_k}$ associated with kBS along with uniform SBS distribution, i.e., $P_{k,D_L}^{r_k}(\gamma_k, U)$ and $P_{k,U_L}^{r_k}(\gamma_k, U)$ are given, respectively, as

$$P_{k,D_L}^{r_k}(\gamma_k, U) = \frac{1}{\exp(-\rho_M \pi r_1^2)} \int_{d_1^{r_k}}^{d_2^{r_k}} \exp\left(\frac{-\gamma_k}{\eta_k}\right) \exp\left(-2\pi\left[\rho_k^r O_k^r + \rho_u^r O_u^r + \rho_\tau^{R(U)} O_\tau^r + \rho_u^r O_u^r\right]\right) \times (2\pi\rho_k y_k \exp(-\rho_k \pi y_k^2)) dy_k, \tag{18}$$

and

$$P_{k,U_L}^{r_k}(\gamma_k, U) = \frac{1}{\exp(-\rho_M \pi r_1^2)} \int_{d_1^{r_k}}^{d_2^{r_k}} \exp\left(\frac{-\gamma_k}{\eta_k}\right) \exp\left(-2\pi\left[\rho_u^r O_u^r + \rho_k^r O_k^r + \rho_u^r O_u^r + \rho_\tau^{R(U)} O_\tau^r\right]\right) \times (2\pi\rho_k y_k \exp(-\rho_k \pi y_k^2)) dy_k, \tag{19}$$

where η_k is the kBS transmitted SNR, and ρ_k and ρ_τ represent the densities of kBS and τBS , respectively. Similarly O_k^r, O_u^r, O_τ^r and O_u^r , are given, respectively, as

$$O_k^r = \int_{d_1^{r_k}}^{d_2^{r_k}} \left(\frac{x_k}{1 + (s\beta P_{t,D_L}^k)^{-1} \|x_k\|^\alpha}\right) dx_k, \tag{20}$$

$$O_u^r = \int_{d_1^{r_k}}^{d_2^{r_k}} \left(\frac{y_k}{1 + (sP_{t,U_L}^u)^{-1} \|y_k\|^\alpha}\right) dy_k, \tag{21}$$

$$O_\tau^r = \int_{0^{r_\tau}}^{d_1^{r_\tau}} \left(\frac{x_\tau}{1 + (sP_{t,D_L}^\tau)^{-1} \|x_\tau\|^\alpha}\right) dx_\tau, \tag{22}$$

and

$$O_u^r = \int_{0^{r_\tau}}^{d_1^{r_\tau}} \left(\frac{y_\tau}{1 + (sP_{t,U_L}^u)^{-1} \|y_\tau\|^\alpha}\right) dy_\tau. \tag{23}$$

Here P_t^k, P_t^τ and P_t^u are the power transmitted by $kBS, \tau BS$ and users, respectively, where $k \in (M, S)$ and $\tau \in (M, S) \forall k \neq \tau$.

3.2 Coverage probability for nonuniform SBS distribution scenario

D_L and U_L coverage probability of $T_u^{r_k}$ associated with kBS , along with nonuniform SBS distribution, $P_{k,D_L}^{r_k}(\gamma_k, NU)$ and $P_{k,U_L}^{r_k}(\gamma_k, NU)$ are given, respectively, as

$$P_{k,D_L}^{r_k}(\gamma_k, NU) = \frac{1}{\exp(-\rho_M \pi r_1^2)} \int_{d_1^{r_k}}^{d_2^{r_k}} \exp\left(\frac{-\gamma_k}{\eta_k}\right) \exp\left(-2\pi\left[\rho_k^r O_k^r + \rho_u^r O_u^r + \rho_\tau^{R(NU)} O_\tau^r + \rho_u^r O_u^r\right]\right) \times (2\pi\rho_k y_k \exp(-\rho_k \pi y_k^2)) dy_k, \tag{24}$$

and

$$P_{k,U_L}^{r_k}(\gamma_k, NU) = \frac{1}{\exp(-\rho_M \pi r_1^2)} \int_{d_1^{r_k}}^{d_2^{r_k}} \exp\left(\frac{-\gamma_k}{\eta_k}\right) \exp\left(-2\pi\left[\rho_u^r O_u^r + \rho_k^r O_k^r + \rho_u^r O_u^r + \rho_\tau^{R(NU)} O_\tau^r\right]\right) \times (2\pi\rho_k y_k \exp(-\rho_k \pi y_k^2)) dy_k, \tag{25}$$

where $\rho_\tau^{R(NU)}$ denotes nonuniform SBS distribution, and O_k^r, O_u^r, O_τ^r and O_u^r are defined, respectively, as

$$O_k^r = \int_{d_1^{r_k}}^{d_2^{r_k}} \left(\frac{x_k}{1 + (s\beta P_{t,D_L}^k)^{-1} \|x_k\|^\alpha}\right) dx_k, \tag{26}$$

$$O_u^r = \int_{d_1^{r_k}}^{d_2^{r_k}} \left(\frac{y_k}{1 + (sP_{t,U_L}^u)^{-1} \|y_k\|^\alpha}\right) dy_k, \tag{27}$$

$$O_\tau^r = \int_{0^{r_\tau}}^{d_1^{r_\tau}} \left(\frac{x_\tau}{1 + (sP_{t,D_L}^\tau)^{-1} \|x_\tau\|^\alpha}\right) dx_\tau, \tag{28}$$

and

$$O_u^r = \int_{0^{r_\tau}}^{d_1^{r_\tau}} \left(\frac{y_\tau}{1 + (sP_{t,U_L}^u)^{-1} \|y_\tau\|^\alpha}\right) dy_\tau. \tag{29}$$

Expressions for coverage probabilities obtained in this section are based on the mathematical preliminaries derived for the SFR scheme in Sect. 2.3. Numerical results for the above expressions are discussed in Sect. 4. Proof of Eq. 24) is given in Appendix.

Table 5 Simulation parameters

Parameter	Configuration/value
BS and user locations	PPPs
Bandwidth of channel	10 MHz
$\rho_M(U)$	6 MBSs/ $(\pi(R(U))^2)$ km ²
$\rho_M(NU)$	3 MBSs/ $(\pi(R(U))^2)$ km ²
$\rho_S(U)$	16 SBSs/ $(\pi(R(U))^2)$ km ²
$\rho_S(NU)$	8 SBSs/ $(\pi(R(U))^2)$ km ²
ρ_u	45 users/ $(\pi(R(U))^2)$ km ²
P_t^M, P_t^S, P_t^u	40 dBm, 20 dBm and 20 dBm, respectively
$\alpha_m = \alpha_s = \alpha$	$2 < \alpha \leq 4$
β	0 dB and 5 dB for (r_k^i, r_τ^i) and (r_k^e, r_τ^e) , respectively.
σ^2	−174 dBm
Spectrum access method	Open access

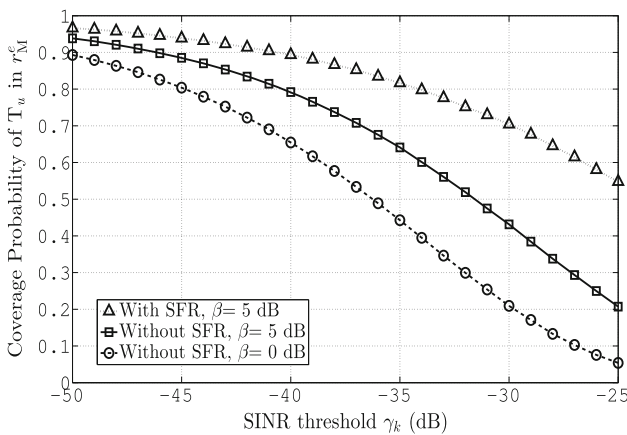


Fig. 4 Coverage probability versus SINR threshold

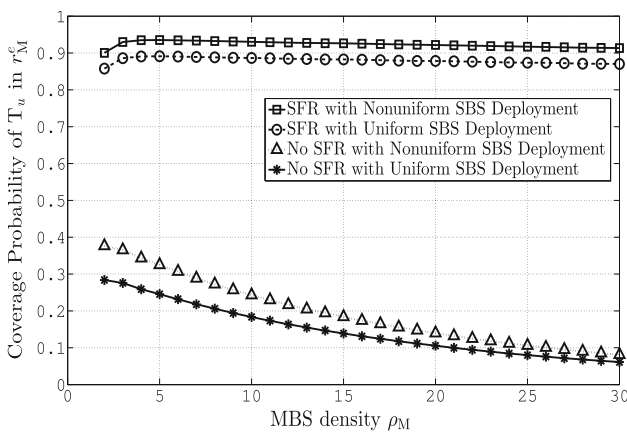


Fig. 5 Coverage probability versus ρ_M

4 Results and discussion

In this section, we provide discussion on different numerical results for the employment of SFR while considering both uniform and nonuniform SBS distribution scenario in

the coverage region of MBS. The results are derived using Matlab (Version 2017a) with parameters listed in Table 5.

Figure 4 presents MBS coverage probability against different values of the SINR thresholds. There are three types of comparisons in this result, i.e., the proposed model is used: (1) with SFR scheme and load balancing, (2) without SFR scheme while considering load balancing, and (3) without SFR scheme and no load balancing. The result demonstrates that increasing SBS power in r_M^e results in improved coverage due to load balancing across the network. Moreover, SFR with $\beta = 5$ dB outperforms rest of the analysis scenarios.

Figure 5 presents coverage probability against ρ_M for uniform and nonuniform SBS distribution scenarios with and without employing SFR. These results are drawn using D_L coverage probability Eqs. (18) and (24) for both uniform and nonuniform SBS deployment scenarios while assuming SINR threshold, $\gamma_k = -25$ dB. We observe significant degradation in the coverage probability when there is no SFR employed. However, with the introduction of

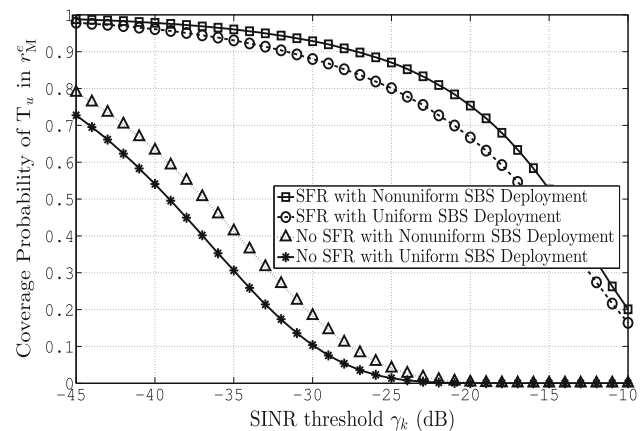


Fig. 6 Coverage probability versus SINR threshold in r_M^e

SFR, our proposed model becomes more resilient to interference and, therefore, coverage probability is notably improved. Furthermore, it can be observed from the figure that nonuniform SBS deployment results in better coverage probability against other aforementioned scenarios. This coverage improvement is due to reduced interference caused by fewer number of active SBSs. It can be deduced from the figure that $\rho_M(NU) \approx 4 - 8 \text{ MBSs}/(\pi(R(U))^2) \text{ km}^2$ gives the optimum coverage for the proposed model.

Figure 6 compares the coverage probability with SINR threshold, γ_k , for the T_u located in r_M^e using Eqs. (18) and (24). The figure also compares uniform and nonuniform SBS distribution scenarios while assuming both SFR and no SFR for interference mitigation with $\rho_M(U) = 6 \text{ MBSs}/(\pi(R(U))^2) \text{ km}^2$, $\rho_M(NU) = 3 \text{ MBSs}/(\pi(R(NU))^2) \text{ km}^2$, $\rho_S(U) = 16 \text{ SBSs}/(\pi(R(U))^2) \text{ km}^2$, $\rho_S(NU) = 8 \text{ SBSs}/(\pi(R(NU))^2) \text{ km}^2$, and $\rho_u(U) = 45 \text{ users}/(\pi(R(U))^2) \text{ km}^2$. The plots show that SFR along with nonuniform SBS deployment has significant impact on interference reduction and, thus, results in improved coverage probability. Furthermore, it can be observed that higher values of γ_k lead to degradation in coverage probability due to reduced user association with k SBS.

In Fig. 7, coverage probability is compared with SNR (MBS signal power affected by noise σ^2). Here $\gamma_k = -25 \text{ dB}$. As depicted in the figure, nonuniform SBS distribution scenario outperforms uniform SBS distribution scenario in terms of better coverage probability for different values of η_k . Furthermore, the results in this figure establish the fact that increasing the value of η_k produces better coverage probability due to reduced interference.

In Fig. 8, coverage probabilities are presented against SBS densities for $\gamma_k = -25 \text{ dB}$, while considering both uniform and nonuniform SBS distribution scenarios. This

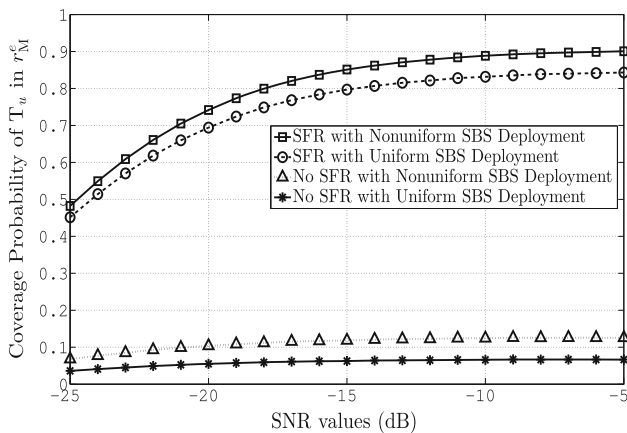


Fig. 7 Coverage probability versus received SNR in r_M^e

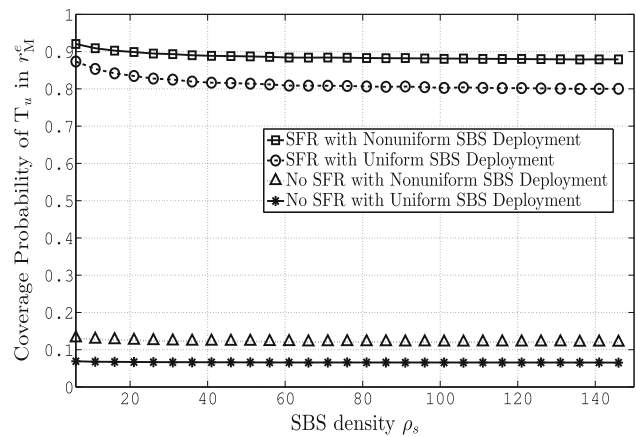


Fig. 8 Coverage probability versus SBS density in r_M^e

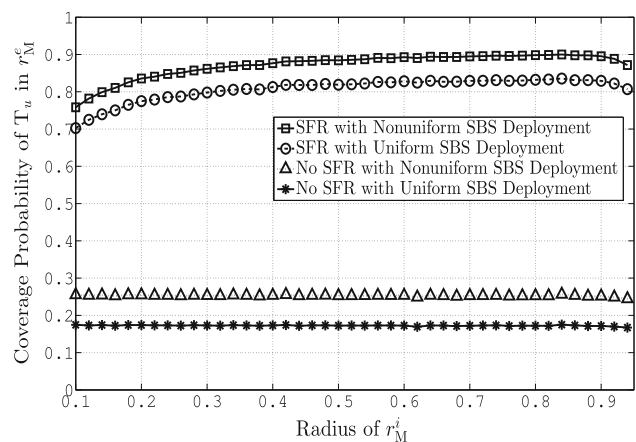


Fig. 9 Coverage probability versus r_M^i radius

figure shows that increasing number of SBSs deployed inside the coverage area of MBS results in decreased coverage probability, which is due to increased interference received from dense SBS deployment. Furthermore, degradation in coverage probability is smaller as compared with Fig. 5. This is due to higher transmitted power by MBS compared with SBS. Here, P_t^M , P_t^S and P_t^u are set to 40 dB, 20 dB and 20 dB, respectively.

Figure 9 compares coverage probability with radius of r_M^i for $\gamma_k = -20 \text{ dB}$. From the figure it can be observed that the optimum value of d_1^i is approximately 70% of d_2^e . It can also be observed from the figure that beyond this point, performance improvement, in terms of coverage probability, degrades. Furthermore, nonuniform SBS deployment with SFR scheme outperforms rest of the simulation scenarios.

5 Conclusion

In ultra-dense SBS deployment, offloading of users from MBS to SBSs in edge coverage region of MBS has a significant impact on SINR degradation due to increased interference received from offloaded MBS users. For interference mitigation, the proposed model considers the SFR scheme along with nonuniform SBS distribution scenario. Expressions for coverage probabilities are derived for both uniform and nonuniform distribution scenarios. Numerical results indicate that the proposed model becomes more resilient to interference by using the SFR scheme. Similarly, analysis of SFR with nonuniform SBS deployment shows significant improvement in coverage probability due to reduced interference and efficient utilization of SBS resources. Results also show that optimum radius for interior coverage region of MBS is about 70% of radius for edge coverage region of MBS. Furthermore, increasing the densities of MBS and SBS adversely affect the coverage probability due to increased interference, while decreasing the value of SINR threshold results in improved coverage due to more number of associated users. As a future direction, this work can be extended to find the most favorable value of β in the proposed model to achieve optimal load balancing among MBS and SBSs.

Appendix

Proof Proof of Eq. (24)

$$P_{k,D_L}^{r_k^e}(\gamma_k, NU) = E \left[P \left[\Gamma_k^{r_k^e}(y_k) > \gamma_k | \mathbf{T}_u^{r_k^e} \right] \right] \tag{30}$$

$$= \int_{d_1^{r_k^e}}^{d_2^{r_k^e}} P \left[\Gamma_k^{r_k^e}(y_k) > \gamma_k | \mathbf{T}_u^{r_k^e} \right] f_{Y_k | \mathbf{T}_u^{r_k^e}}(y_k) dy_k,$$

where Γ_k and γ_k are, respectively, the SINR and its threshold for k BBS. $P[\Gamma_k^{r_k^e}(y_k) > \gamma_k | \mathbf{T}_u^{r_k^e}]$ denotes the success probability, which is defined as the received SINR greater than γ_k at $\mathbf{T}_u^{r_k^e}$, while associated with k BBS. It can be further written as

$$P[\Gamma_k^{r_k^e}(y_k) > \gamma_k | \mathbf{T}_u^{r_k^e}] \tag{31}$$

$$\stackrel{i}{=} E_{I_{tot,D_L}^{r_k^e}(NU)} \left[\left(\frac{P_k h_r r^{-\alpha}}{I_{tot,D_L}^{r_k^e}(NU) + \sigma^2} \right) > \gamma_k | \mathbf{T}_u^{r_k^e} \right]$$

$$\stackrel{ii}{=} \exp \left(\frac{-\gamma_k}{\eta_k} \right) E_{I_{tot,D_L}^{r_k^e}(NU)} \left[\exp(-s I_{tot,D_L}^{r_k^e}(NU)) \right]$$

$$\stackrel{iii}{=} \exp \left(\frac{-\gamma_k}{\eta_k} \right) M_{I_{tot,D_L}^{r_k^e}(NU)}(s),$$

where $I_{tot,D_L}^{r_k^e}(NU)$ is the total interference received at $\mathbf{T}_u^{r_k^e}$

associated with k BBS, and $s = \frac{\gamma_k ||y_k||^\alpha}{P_{r,k}}$. Step (i) is obtained by substituting the value of η_k . Similarly, we obtain step (ii) by substituting Eqs. (3) into (31), using independence of interferences, and Nakagami-m fading assumption for all the links. In Step (iii), $M_{I_{tot,D_L}^{r_k^e}(NU)}(s)$ is the moment generating functional (MGF) [15] of $I_{tot,D_L}^{r_k^e}(NU)$. Using Eq. (11), $M_{I_{tot,D_L}^{r_k^e}(NU)}(s)$ can be calculated as

$$M_{I_{tot,D_L}^{r_k^e}(NU)}(s) \stackrel{iv}{=} E_{(\Psi_k^{r_k^e} \setminus d_k, \Psi_u^{r_k^e}, \Psi_\tau^{R(NU)}, \Psi_\tau^{r_k^e}, h_{x_k}^{r_k^e}, h_{x_k}^{r_k^e}, h_{y_\tau}^{r_k^e}, h_{y_\tau}^{r_k^e})} \left[\exp \left(-s \left(\sum_{x_k \in \Psi_k^{r_k^e} \setminus d_k} \beta P_{t,D_L}^k h_{x_k}^{r_k^e} ||x_k||^{-\alpha} + \sum_{y_k \in \Psi_u^{r_k^e}} P_{t,U_L}^u h_{y_k}^{r_k^e} ||y_k||^{-\alpha} + \sum_{x_\tau \in \Psi_\tau^{R(NU)}} P_{t,D_L}^r h_{x_\tau}^{r_k^e} ||x_\tau||^{-\alpha} + \sum_{y_\tau \in \Psi_\tau^{r_k^e}} P_{t,U_L}^u h_{y_\tau}^{r_k^e} ||y_\tau||^{-\alpha} \right) \right) \right], \tag{32}$$

where $E_{(\Psi_k^{r_k^e} \setminus d_k, \Psi_u^{r_k^e}, \Psi_\tau^{R(NU)}, \Psi_\tau^{r_k^e}, h_{x_k}^{r_k^e}, h_{x_k}^{r_k^e}, h_{y_\tau}^{r_k^e}, h_{y_\tau}^{r_k^e})}[\cdot]$ denotes the expected value of interference with respect to PPPs and fading coefficients, and $\Psi_k^{r_k^e} \setminus d_k$, $\Psi_u^{r_k^e}$, $\Psi_\tau^{R(NU)}$ and $\Psi_\tau^{r_k^e}$ represent the distribution of BSs and users using PPP in r_k^e and r_τ^i , respectively. By using Nakagami-m fading coefficients for channel estimation and independence assumptions of the PPPs, Step (iv) can be obtained. Further simplification of Eq. (32) leads to

$$M_{I_{tot,D_L}^{r_k^e}(NU)}(s) = \exp \left(-2\pi \rho_k^{r_k^e} \int_{d_1^{r_k^e}}^{d_2^{r_k^e}} \left\{ 1 - M_{h_{x_k}^{r_k^e}}(\beta P_{t,D_L}^k h_{x_k}^{r_k^e} ||x_k||^{-\alpha}) \right\} x_k dx_k \right) \times \exp \left(-2\pi \rho_u^{r_k^e} \int_{d_1^{r_k^e}}^{d_2^{r_k^e}} \left\{ 1 - M_{h_{y_k}^{r_k^e}}(P_{t,U_L}^u h_{y_k}^{r_k^e} ||y_k||^{-\alpha}) \right\} y_k dy_k \right) \times \exp \left(-2\pi \rho_\tau^{R(NU)} \int_{0^{r_\tau^i}}^{d_1^{r_\tau^i}} \left\{ 1 - M_{h_{x_\tau}^{r_k^e}}(P_{t,D_L}^r h_{x_\tau}^{r_k^e} ||x_\tau||^{-\alpha}) \right\} x_\tau dx_\tau \right) \times \exp \left(-2\pi \rho_u^{r_\tau^i} \int_{0^{r_\tau^i}}^{d_1^{r_\tau^i}} \left\{ 1 - M_{h_{y_\tau}^{r_k^e}}(P_{t,U_L}^u h_{y_\tau}^{r_k^e} ||y_\tau||^{-\alpha}) \right\} y_\tau dy_\tau \right). \tag{33}$$

Here $d_1^{r_k^e}$ and $d_2^{r_k^e}$ define the lower and higher limits of r_k^e , while $0^{r_\tau^i}$ and $d_1^{r_\tau^i}$ define the lower and higher boundaries of r_τ^i , respectively. $\{M_{h_{x_k}^{r_k^e}}(\cdot), M_{h_{y_k}^{r_k^e}}(\cdot)\}$ and $\{M_{h_{x_\tau}^{r_k^e}}(\cdot), M_{h_{y_\tau}^{r_k^e}}(\cdot)\}$ are the sets of MGF with respect to fading coefficients for r_k^e and r_τ^i , respectively. Moreover, using the Nakagami-m

fading assumption, a simplified form of Eq. (33) can be written as

$$\begin{aligned}
 & M_{I_{tot,D_L}^{r_k^e}(NU)}(s) \\
 &= \exp\left(-2\pi\rho_k^{r_k^e} \int_{d_1^{r_k^e}}^{d_2^{r_k^e}} \left(\frac{x_k}{1 + (s\beta P_{t,D_L}^k)^{-1} \|x_k\|^\alpha}\right) dx_k\right) \\
 &\times \exp\left(-2\pi\rho_u^{r_k^e} \int_{d_1^{r_k^e}}^{d_2^{r_k^e}} \left(\frac{y_k}{1 + (sP_{t,U_L}^\mu)^{-1} \|y_k\|^\alpha}\right) dy_k\right) \\
 &\times \exp\left(-2\pi\rho_\tau^{R(NU)} \int_{0^{r_\tau^i}}^{d_\tau^{r_\tau^i}} \left(\frac{x_\tau}{1 + (sP_{t,D_L}^\tau)^{-1} \|x_\tau\|^\alpha}\right) dx_\tau\right) \\
 &\times \exp\left(-2\pi\rho_u^{r_\tau^i} \int_{0^{r_\tau^i}}^{d_\tau^{r_\tau^i}} \left(\frac{y_\tau}{1 + (sP_{t,U_L}^\mu)^{-1} \|y_\tau\|^\alpha}\right) dy_\tau\right). \tag{34}
 \end{aligned}$$

Equation (34) can be rewritten as

$$\begin{aligned}
 & M_{I_{tot,D_L}^{r_k^e}(NU)}(s) \\
 &= \exp\left(-2\pi\left[\rho_k^{r_k^e} O_k^{r_k^e} + \rho_u^{r_k^e} O_u^{r_k^e} + \rho_\tau^{R(NU)} O_\tau^{r_\tau^i} + \rho_u^{r_\tau^i} O_u^{r_\tau^i}\right]\right), \tag{35}
 \end{aligned}$$

where

$$O_k^{r_k^e} = \int_{d_1^{r_k^e}}^{d_2^{r_k^e}} \left(\frac{x_k}{1 + (s\beta P_{t,D_L}^k)^{-1} \|x_k\|^\alpha}\right) dx_k, \tag{36}$$

$$O_u^{r_k^e} = \int_{d_1^{r_k^e}}^{d_2^{r_k^e}} \left(\frac{y_k}{1 + (sP_{t,U_L}^\mu)^{-1} \|y_k\|^\alpha}\right) dy_k, \tag{37}$$

$$O_\tau^{r_\tau^i} = \int_{0^{r_\tau^i}}^{d_\tau^{r_\tau^i}} \left(\frac{x_\tau}{1 + (sP_{t,D_L}^\tau)^{-1} \|x_\tau\|^\alpha}\right) dx_\tau, \tag{38}$$

and

$$O_u^{r_\tau^i} = \int_{0^{r_\tau^i}}^{d_\tau^{r_\tau^i}} \left(\frac{y_\tau}{1 + (sP_{t,U_L}^\mu)^{-1} \|y_\tau\|^\alpha}\right) dy_\tau. \tag{39}$$

Substituting Eqs. (35) into (31), the success probability that Γ_k is greater than γ_k can be obtained as

$$\begin{aligned}
 & P[\Gamma_k^{r_k^e}(y_k) > \gamma_k | T_u^{r_k^e}] = \exp\left(\frac{-\gamma_k}{\eta_k}\right) \\
 &\times \exp\left(-2\pi\left[\rho_k^{r_k^e} O_k^{r_k^e} + \rho_u^{r_k^e} O_u^{r_k^e} + \rho_\tau^{R(NU)} O_\tau^{r_\tau^i} + \rho_u^{r_\tau^i} O_u^{r_\tau^i}\right]\right). \tag{40}
 \end{aligned}$$

Finally, we obtain Eq. (24) by substituting Eqs. (17) and (40) into (30).

Similarly, proof of Eq. (18) can be obtained by using the same approach as for the proof of Eq. (24). \square

References

1. Haroon, M. S., Abbas, Z. H., Abbas, G., & Muhammad, F. (2018). Analysis of interference mitigation in heterogeneous cellular networks using soft frequency reuse and load balancing. In *28th international telecommunication networks and applications conference (ITNAC)* (pp. 1–6).
2. Adejo, A., Boussakta, S., & Neasham, J. (2017). Interference modeling for soft frequency reuse in irregular heterogeneous cellular networks. In *Ninth international conference on ubiquitous and future networks (ICUFN)* (pp. 381–386).
3. Zhang, H., Jiang, C., Hu, R. Q., & Qian, Y. (2016). Self-organization in disaster-resilient heterogeneous small cell networks. *IEEE Network*, *30*(2), 116–121.
4. Jiang, X., Zheng, B., Zhu, W. P., Wang, L., & Zou, Y. (2018). Large system analysis of heterogeneous cellular networks with interference alignment. *IEEE Access*, *6*, 8148–8160.
5. Muhammad, F., Abbas, Z. H., & Li, F. Y. (2017). Cell association with load balancing in nonuniform heterogeneous cellular networks: Coverage probability and rate analysis. *IEEE Transactions on Vehicular Technology*, *66*(6), 5241–5255.
6. Lei, J., Chen, H., & Zhao, F. (2018). Stochastic geometry analysis of downlink spectral and energy efficiency in ultradense heterogeneous cellular networks. *Mobile Information Systems*, 2018. <https://doi.org/10.1155/2018/1684128>
7. Zhang, H., Dong, Y., Cheng, J., Hossain, M. J., & Leung, V. C. (2016). Fronthauling for 5G LTE-U ultra dense cloud small cell networks. *IEEE Wireless Communications*, *23*(6), 48–53.
8. Wang, Y., & Pedersen, K. I. (2012). Performance analysis of enhanced inter-cell interference coordination in LTE-Advanced heterogeneous networks. In *Vehicular Technology Conference (VTC)* (pp. 1–5).
9. Lee, P., Lee, T., Jeong, J., & Shin, J. (2010). Interference management in LTE femtocell systems using fractional frequency reuse. In *Advanced communication technology (ICACT)* (pp. 1047–1051).
10. Saquib, N., Hossain, E., & Kim, D. I. (2013). Fractional frequency reuse for interference management in LTE-advanced hetnets. *IEEE Wireless Communications*, *20*(2), 113–122.
11. Pervez, M. M., Abbas, Z. H., Muhammad, F., & Jiao, L. (2016). Location-based coverage and capacity analysis of a two tier HetNet. *IET Communications*, *11*(7), 1067–1073.
12. Abbas, Z. H., Muhammad, F., & Jiao, L. (2017). Analysis of load balancing and interference management in heterogeneous cellular networks. *IEEE Access*, *5*, 14690–14705.
13. Novlan, T. D., Ganti, R. K., Ghosh, A., & Andrews, J. G. (2012). Analytical evaluation of fractional frequency reuse for heterogeneous cellular networks. *IEEE Transactions on Communications*, *60*(7), 2029–2039.

14. Guo, L., Cong, S., & Sun, Z. (2017). Multichannel analysis of soft frequency reuse and user association in two-tier heterogeneous cellular networks. *EURASIP Journal on Wireless Communications and Networking*, 2017(1), 168.
15. Fereydooni, M., Sabaei, M., Dehghan, M., Eslamlou, G. B., & Rupp, M. (2018). Analytical evaluation of heterogeneous cellular networks under flexible user association and frequency reuse. *Computer Communications*, 116, 147–158.
16. Muhammad, F., Abbas, Z. H., & Jiao, L. (2016). Analysis of interference avoidance with load balancing in heterogeneous cellular networks. In *Personal, indoor, and mobile radio communications (PIMRC)* (pp. 1–6).
17. Baccelli, F., & Blaszczyszyn, B. (2010). Stochastic geometry and wireless networks: Volume II applications. *Foundations and Trends in Networking*, 4(1–2), 1–312.
18. Rosa, C., Pedersen, K., Wang, H., Michaelsen, P. H., Barbera, S., Malkamaki, E., et al. (2016). Dual connectivity for LTE small cell evolution: Functionality and performance aspects. *IEEE Communications Magazine*, 54(6), 137–143.
19. Zhang, H., Huang, S., Jiang, C., Long, K., Leung, V. C., & Poor, H. V. (2017). Energy efficient user association and power allocation in millimeter-wave-based ultra dense networks with energy harvesting base stations. *IEEE Journal on Selected Areas in Communications*, 35(9), 1936–1947.
20. Simon, M. K., & Alouini, M. S. (1998). A unified approach to the performance analysis of digital communication over generalized fading channels. *Proceedings of the IEEE*, 86(9), 1860–1877.
21. Wang, H., Zhou, X., & Reed, M. C. (2013). Analytical evaluation of coverage-oriented femtocell network deployment. In: *International conference on communications (ICC)* (pp. 5974–5979).
22. Chiu, S. N., Stoyan, D., Kendall, W. S., & Mecke, J. (2013). *Stochastic geometry and its applications*. Hoboken: Wiley.
23. Singh, S., & Andrews, J. G. (2014). Joint resource partitioning and offloading in heterogeneous cellular networks. *IEEE Transactions on Wireless Communications*, 13(2), 888–901.
24. Dhillon, H. S., Ganti, R. K., Baccelli, F., & Andrews, J. G. (2012). Modeling and analysis of K-tier downlink heterogeneous cellular networks. *IEEE Journal on Selected Areas in Communications*, 30(3), 550–560.
25. Wang, H., Zhou, X., & Reed, M. C. (2013). Analytical evaluation of coverage-oriented femtocell network deployment. In *International conference on communications (ICC)* (pp. 5974–5979).
26. Andrews, J. G., Baccelli, F., & Ganti, R. K. (2011). A tractable approach to coverage and rate in cellular networks. *IEEE Transactions on Communications*, 59(11), 3122–3134.



Muhammad Sajid Haroon received the B.Sc. degree in electronics engineering from International Islamic University Islamabad, Pakistan, in 2007, and M.S. degrees in electrical engineering from COMSATS Institute of Information Technology, Attock, Pakistan, in 2013. He is currently pursuing the Ph.D. degree with the Ghulam Ishaq Khan Institute of Engineering Science and Technology, Swabi, Pakistan, with a focus on Interference manage-

ment in next generation cellular networks using tools from stochastic geometry, point process theory, and spatial statistics. His research interests include interference mitigation in cellular networks, next

generations cellular networks, stochastic processes and digital signal processing.



Ziaul Haq Abbas received the M.Phil. degree in electronics from Quaid-e-Azam University, Pakistan, in 2001, and the Ph.D. degree from the Agder Mobility Laboratory, Department of Information and Communication Technology, University of Agder, Norway, in 2012. He joined the Ghulam Ishaq Khan (GIK) Institute of Engineering Sciences and Technology, Pakistan, as a Research Associate. In 2012, he was a Visiting

Researcher with the Department of Electrical and Computer Engineering, University of Minnesota, USA. He is currently an Associate Professor with the Faculty of Electrical Engineering and a co-founding member of the Telecommunications and Networking (TeleCoN) Research Lab at GIK Institute. His research interests include energy efficiency in hybrid mobile and wireless communication networks, 4G and beyond mobile systems, mesh and ad hoc networks, traffic engineering in wireless networks, performance evaluation of communication protocols and networks by analysis and simulation, quality-of-service in wireless networks, green wireless communication, and cognitive radio.



Ghulam Abbas received the B.S. degree in computer science from University of Peshawar, Pakistan, in 2003, and the M.S. degree in distributed systems and the Ph.D. degree in computer networks from the University of Liverpool, UK, in 2005 and 2010, respectively. From 2006 to 2010, he was Research Associate with Liverpool Hope University, UK, where he was associated with the Intelligent and Distributed Systems Laboratory. Since

2011, he has been with the Faculty of Computer Sciences and Engineering, GIK Institute of Engineering Sciences and Technology, Pakistan. He is currently working as Associate Professor and Director Huawei Authorised Information and Network Academy. He is a co-founding member of the Telecommunications and Networking (TeleCoN) Research Lab at GIK Institute. Dr. Abbas is a Fellow of the Institute of Science and Technology, UK, a Fellow of the British Computer Society, and a Senior Member of the IEEE. His research interests include computer networks and wireless and mobile communications.



Fazal Muhammad received the B.Sc. and M.Sc. degrees in electrical engineering from the University of Engineering and Technology, Peshawar, Pakistan, in 2004 and 2007, respectively, and the Ph.D. degree in electronic engineering from GIK Institute of Engineering Sciences and Technology, Pakistan in 2017. He is currently working as Assistant Professor and Head of Electrical Engineering Department at City University of Sciences and

Information Technology, Peshawar. He is the Secretary of Institutions

of Engineers, Pakistan, Peshawar Center. His research interests include heterogeneous cellular networks, cognitive radio networks, and sensor networks.

Publisher's Note Springer Nature remains neutral with regard to jurisdictional claims in published maps and institutional affiliations.